Published Online: 2026 May 5 **Research Article**

HTLV-1 Tax Transcriptionally Activates HMGB1 and Links Glycolytic Reprogramming to Immune-Evasion Phenotypes in Adult T-Cell Leukemia/Lymphoma

Ruoting Lin [1], Shuang Zhou [2], Hongzhi Gao [3, *], Ruoteng Xie [2, **]

[1] Department of Neurology, The Second Affiliated Hospital, Fujian Medical University, Quanzhou, Fujian, China
[2] Department of Laboratory Medicine, The Second Affiliated Hospital, Fujian Medical University, Quanzhou, Fujian, China
[3] Department of Neurosurgery, Clinic Center of Molecular Diagnosis and Therapy, The Second Affiliated Hospital, Fujian Medical University, Quanzhou, Fujian, China

[*] ***Corresponding Author:*** Department of Neurosurgery, Clinic Center of Molecular Diagnosis and Therapy, The Second Affiliated Hospital, Fujian Medical University, Quanzhou, Fujian, China. Email: 13559040780@163.com
[**] ***Corresponding Author:*** Department of Laboratory Medicine, The Second Affiliated Hospital, Fujian Medical University, Quanzhou, Fujian, China. Email: 13358597699@163.com

Received: 23 March, 2026; **Revised:** 3 April, 2026; **Accepted:** 5 April, 2026

Abstract

Background: Adult T-cell leukemia/lymphoma (ATLL) is a human T-cell leukemia virus type 1 (HTLV-1)-associated T-cell malignancy marked by metabolic remodeling and immune escape. Whether the viral transactivator Tax directly engages host transcriptional regulators that connect these processes remains unclear.

Objectives: This study tested whether Tax transcriptionally activates high mobility group box 1 (HMGB1) and whether the Tax-HMGB1 axis is associated with glycolytic and immune-evasion phenotypes in ATLL.

Methods: Public Gene Expression Omnibus (GEO) cohorts were analyzed within cohort after dataset-specific preprocessing, probe-to-gene collapsing, and standardized signature scoring. Patient-cohort findings were interpreted as associations, whereas mechanistic ordering was examined in a Tax-inducible T-cell model by HMGB1 promoter luciferase assays, chromatin immunoprecipitation quantitative polymerase chain reaction (ChIP-qPCR), small interfering RNA (siRNA) knockdown/rescue, extracellular acidification rate (ECAR), lactate and glucose-uptake assays, flow cytometry, and donor-matched cytotoxic co-culture.

Results: In ATLL samples, HMGB1 expression and predefined glycolysis and immune-inhibitory signature scores were higher than in normal CD4+ T-cell controls. Within ATLL, HMGB1 expression was positively associated with both scores and with programmed death-ligand 1 (PD-L1; CD274). Tax induction in a switch model increased HMGB1 expression together with glycolytic and checkpoint-related programs. In mechanistic assays, Tax increased HMGB1 promoter activity and enriched the HMGB1 promoter interval -1163 to -975 in ChIP-qPCR, whereas mutation of a C/EBP-like motif blunted reporter responsiveness. HMGB1 knockdown reduced lactate, ECAR, glucose uptake, PD-L1 and Galectin-9 surface expression, and resistance to cytotoxic killing; HMGB1 re-expression partially restored metabolic output. Lactate inhibition and PD-L1 blockade each partially rescued cytotoxic killing in donor-matched co-cultures.

Conclusions: The experimental data support direct transcriptional activation of HMGB1 by Tax and place HMGB1 upstream of a lactate-associated immune-evasion phenotype in ATLL models. The public patient datasets provide complementary associative support but do not by themselves establish causality or resolve contributions from extracellular HMGB1 and tumor microenvironmental composition.

Keywords: HTLV-1, Tax, HMGB1, adult T-cell leukemia/lymphoma, glycolysis, lactate, PD-L1, immune evasion

1. Introduction

Adult T-cell leukemia/lymphoma (ATLL) is a mature T-cell neoplasm caused by chronic infection with human T-cell leukemia virus type 1 (HTLV-1) (1). ATLL remains difficult to treat, and its pathobiology reflects long-term virus-host co-evolution that alters transcriptional control, nutrient utilization, and immune surveillance (1).

The HTLV-1 transactivator Tax is critical for early transformation and can continue to influence tumor-cell states even when its expression becomes intermittent in vivo under immune pressure (2, 3). Tax cooperates with host transcription factors and co-activators to remodel chromatin and to drive proliferative, inflammatory, and pro-survival transcriptional programs (4). Because those programs can affect both cellular metabolism and immune

How to Cite: Lin R, Zhou S, Gao H, Xie R. HTLV-1 Tax Transcriptionally Activates HMGB1 and Links Glycolytic Reprogramming to Immune-Evasion Phenotypes in Adult T-Cell Leukemia/Lymphoma. Jundishapur J Microbiol. 2026;19(4):e171048. doi: https://doi.org/10.5812/jjm-171048

signaling, Tax is a plausible upstream regulator of immunometabolic adaptation in ATLL (4, 5).

High mobility group box 1 (HMGB1) is a chromatin-associated DNA-binding protein with distinct nuclear transcriptional functions and extracellular immunomodulatory activities (6). In cancer, intracellular HMGB1 can support tumor-cell fitness, whereas extracellular HMGB1 can reshape immune-cell behavior in the tumor microenvironment (6). How Tax-driven transcriptional control intersects with HMGB1, glycolysis, lactate accumulation, and immune-evasion phenotypes in ATLL has not been systematically resolved (7 - 9).

Here we used a multi-layer strategy integrating public transcriptomes with targeted functional assays to test a bounded working model: Tax transcriptionally activates HMGB1, and HMGB1 in turn supports a glycolytic, lactate-rich state that contributes to immune-evasion phenotypes in ATLL (4 - 6, 8 - 10). We explicitly distinguish observational cohort analyses from causal tests performed in the Tax-switch, promoter, and HMGB1 perturbation models.

An overview of the study design and working model is shown in Figure 1.

2. Methods

2.1. Public Transcriptome Datasets and Cohort Annotation

Three public Gene Expression Omnibus (GEO) datasets were used for bulk-transcriptome discovery and one single-cell dataset was used for cell-type context: GSE33615 (ATLL vs normal controls), GSE10508 (Tax-on vs Tax-off), GSE17718 (HTLV-1-positive vs HTLV-1-negative comparison cohort), and GSE195674 (supporting single-cell ATLL dataset). Sample annotations were curated from GEO series matrices or sample tables and harmonized into a study manifest containing cohort label, biological group, platform, sample source, and analysis role (Table 1).

2.2. Preprocessing and Dataset Harmonization

For the bulk datasets, we imported the processed expression values distributed by GEO rather than pooling raw files across platforms. Array intensities were retained on the native processed scale supplied by each series; when necessary for comparability, values were transformed to the log2 scale after inspection of range and density. Platform annotations were used to map probes to HGNC gene symbols. When multiple probes mapped to the same gene within a dataset, the probe with the highest mean expression was retained. Unannotated probes and invariant features were excluded from unsupervised analyses. Because GSE33615, GSE10508, and GSE17718 differ in platform and source material, absolute expression was interpreted only within cohort, whereas cross-cohort comparisons were based on within-cohort log2 fold changes and standardized signature scores.

2.3. Gene-Level Quantification and Predefined Signature Scores

HMGB1 and CD274 expression values were examined at gene level. To reduce overreliance on single-gene readouts, we also quantified a glycolysis signature score and an immune-inhibitory signature score. The glycolysis score summarized SLC2A1, HK2, PFKP, ALDOA, PDK1, PKM, and LDHA. The immune-inhibitory score summarized CD274, LGALS9, IDO1, CTLA4, TIGIT, LAG3, and TGFB1. For each cohort, gene-level expression values were centered and scaled, and signature scores were calculated as the mean z score of the genes in the relevant set. Standardized scores were used for plots and correlation analyses so that results reflected within-cohort relative enrichment rather than cross-platform absolute intensity. Exact gene-set composition and analysis metadata are included in the reproducibility package accompanying the revised submission.

2.4. Differential Expression and Effect-Size Concordance

We analyzed a focused panel of 26 axis-related genes as prespecified mechanistic candidates rather than claiming unbiased genome-wide discovery. Within each cohort, differential expression between groups was summarized as log2 fold change and Benjamini-Hochberg false discovery rate (FDR)-adjusted P values. Directional concordance across cohorts was assessed by comparing the sign and magnitude of log2 fold changes for the same candidate genes (Supplementary Figure S5; Supplementary Tables S1-S4).

2.5. Correlation, Regression, and Interpretive Boundaries for Bulk Cohorts

Associations among HMGB1, glycolysis, immune-inhibitory signaling, and CD274 were evaluated in the ATLL cohort using Spearman correlation. We also fit linear models with dataset source variables available in the sample annotations as covariates to confirm that the direction of association was not driven solely by source labels. Because diagnosis, tumor burden, and sample composition cannot be fully disentangled in public bulk datasets, these analyses were interpreted as associative. Causal ordering was therefore not inferred from patient

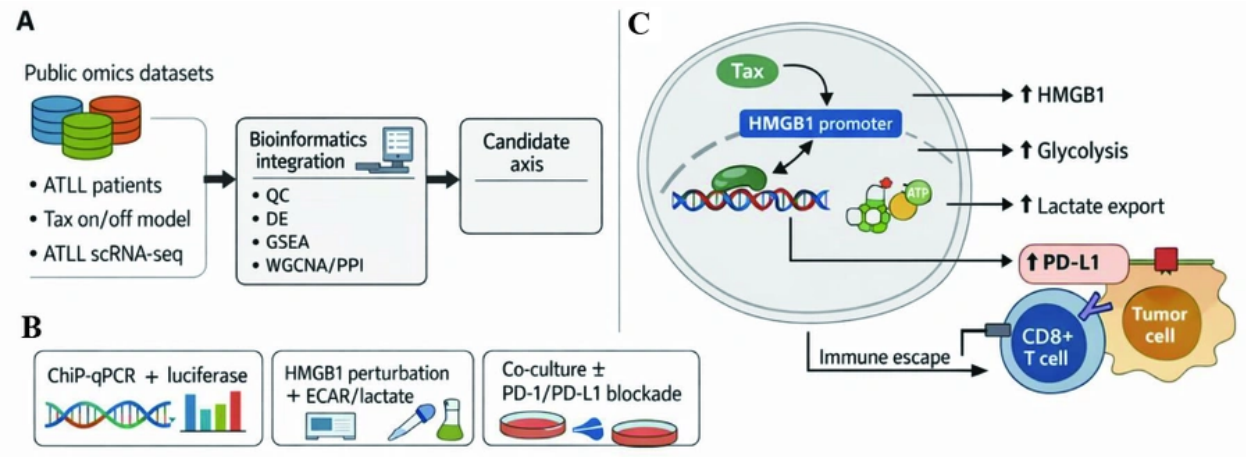

Figure 1. Integrated study design and bounded working model of the Tax-HMGB1 axis in adult T-cell leukemia/lymphoma (ATLL). A, Public Gene Expression Omnibus (GEO) datasets were used for cohort-level analyses of HMGB1, glycolysis, and immune-inhibitory signatures; B, weighted gene co-expression network analysis (WGCNA) and supporting single-cell analyses were used to assign module- and cell-type context; C, a Tax-inducible T-cell model was used for promoter assays, HMGB1 perturbation and rescue, metabolic phenotyping, flow cytometry, and donor-matched immune co-culture. Solid arrows indicate experimentally supported ordering (Tax to HMGB1 and HMGB1 to glycolytic output); dashed arrows indicate associations or partially supported links (lactate to checkpoint expression and tumor-cell state to immune-evasion phenotype). This figure is schematic and was not subjected to statistical testing.

Table 1. Public Datasets Used in This Study

Dataset	Role in study	Samples (n)	Platform and sample type
GSE33615	Discovery ATLL cohort (ATLL vs normal controls)	52 ATLL; 21 normal (total 73)	GPL4133 Agilent whole-genome microarray; ATLL PBMC-derived samples and normal CD4+ T cells
GSE10508	Tax-switch directionality model (Tax-on vs Tax-off)	6 Tax-on; 6 Tax-off (total 12)	GPL570 Affymetrix Human Genome U133 Plus 2.0 Array; Tax-inducible human T-cell model
GSE17718	Effect-size directionality cohort (HTLV-1-positive vs HTLV-1-negative comparison)	3 HTLV-1+; 3 HTLV-1- (total 6)	GPL570 Affymetrix Human Genome U133 Plus 2.0 Array; HTLV-1-positive cell lines and HTLV-1-negative CD4+ comparison samples
GSE195674	Single-cell contextual support	2 samples; 15,981 cells	GPL24676 Illumina NovaSeq 6000 / 10x Genomics 5' single-cell RNA-seq; ATLL skin biopsy-derived cells

Abbreviations: GEO, Gene Expression Omnibus; ATLL, adult T-cell leukemia/lymphoma; PBMC, peripheral blood mononuclear cell; HTLV-1, human T-cell leukemia virus type 1; scRNA-seq, single-cell RNA sequencing.

cohorts alone and was instead tested in the Tax-switch and perturbation experiments.

2.6. Weighted Gene Co-expression Network Analysis

Weighted gene co-expression network analysis (WGCNA) was used to identify modules associated with HMGB1 expression and the two predefined signature scores. A signed network was built from the bulk ATLL cohort using PyWGCNA, with data-driven soft-threshold selection and module merging according to eigengene similarity. Module-trait relationships were summarized by Spearman correlations between module eigengenes and HMGB1 expression, glycolysis score, and immune-inhibitory score. Hub genes and module-trait statistics are reported in Supplementary Tables S5-S7.

2.7. Single-Cell Transcriptome Context

To assign likely cellular context to the bulk associations, we summarized GSE195674 at the level of annotated cell types. Cell-type average log-expression values were computed for HMGB1, the glycolysis signature, CD274, LGALS9, HK2, and LDHA. These analyses were used to localize expression patterns across malignant T cells and tumor-microenvironmental populations, not to make causal inferences.

2.8. Cell Model and Culture Conditions

Mechanistic experiments were performed in a Tax-inducible human T-cell system maintained under

standard culture conditions. Tax-off and Tax-on states were defined by the established switch system used throughout the manuscript. Unless otherwise stated, wet-lab assays were conducted in three independent biological experiments. Experimental condition assignment was determined by the predefined Tax/HMGB1 manipulation; no formal randomization or blinding was applied.

2.9. HMGB1 Promoter Reporter Assays

Wild-type full-length and truncated HMGB1 promoter reporters containing the Tax-responsive interval were cloned upstream of firefly luciferase. The key C/EBP-like motif within the responsive region (-1088 to -1076 within the enriched -1163 to -975 interval) was mutated from TTGCAGCAAAGG to TTGCAttAAAtG to test motif dependence (Supplementary Table S17). Cells were co-transfected with a Renilla luciferase normalization control, and relative activity was reported as firefly/Renilla normalized to the Tax-negative wild-type full-length construct. Each condition was measured in three independent experiments.

2.10. Chromatin Immunoprecipitation Quantitative Polymerase Chain Reaction

Chromatin immunoprecipitation quantitative polymerase chain reaction (ChIP-qPCR) was performed in the Tax-inducible system using an anti-Tax antibody together with matched IgG negative-control immunoprecipitation. qPCR amplicons targeted the HMGB1 promoter interval -1163 to -975, a distal negative-control region, and the NFKBIA promoter as a positive-control Tax-responsive locus (Supplementary Table S18). Enrichment was calculated as IgG-normalized fold enrichment. Positive-control recovery at NFKBIA and minimal signal at the distal negative-control region were used as internal validity checks for antibody specificity and assay performance.

2.11. HMGB1 Perturbation and Metabolic Assays

HMGB1 was knocked down with siRNA in Tax-off and Tax-on states, and a rescue condition was generated by HMGB1 re-expression after knockdown. Primary metabolic endpoints were extracellular lactate concentration, ECAR, and glucose uptake. qPCR and immunoblot validation of glycolysis- and immune-related readouts are provided in Supplementary Figure S4 and Supplementary Tables S12-S14.

2.12. Flow Cytometry and Donor-Matched Immune Co-culture Assays

For immune co-culture experiments, five independent healthy adult donor blood samples were collected after written informed consent. Peripheral blood mononuclear cells were isolated from each donation and activated to generate cytotoxic effector preparations. Each donor-derived effector preparation was tested in parallel against all target-cell conditions, allowing paired donor-level analysis. Target and effector cells were co-cultured at an effector:target ratio of 5:1 for 24 h, a condition chosen to preserve dynamic range in the killing assay. Target-cell killing was defined as the percentage loss of viable target cells relative to paired target-only controls. Supernatant interferon-gamma (IFN-gamma) and lactate were quantified after co-culture. In selected Tax-on conditions, either a PD-L1 blocking antibody or a lactate inhibitor was added to test pathway sensitivity. Surface PD-L1 and Galectin-9 were quantified on target cells as mean fluorescence intensity (MFI) by flow cytometry. Individual donor values are provided in Supplementary Tables S15 and S16.

2.13. Primary Outcomes, Multiplicity, and Statistics

The prespecified primary mechanistic endpoints were HMGB1 promoter activation, HMGB1 promoter occupancy by Tax, and the metabolic readouts lactate, ECAR, and glucose uptake. The prespecified primary functional endpoints were target-cell PD-L1 MFI and donor-matched target-cell killing. Other readouts, including Galectin-9 and IFN-gamma, were considered supportive. Two-group bulk-cohort comparisons used two-sided Mann-Whitney U tests when distributional assumptions were uncertain. Tax-switch and other wet-lab comparisons used two-sided Welch's t-tests unless donor matching required paired t-tests. Correlations used Spearman's rho. FDR correction was applied within the candidate-gene differential-expression analyses for each cohort. Because the wet-lab endpoints were hypothesis-driven and hierarchically organized around the primary endpoints above, no across-assay omnibus multiplicity correction was applied; supportive endpoints were interpreted accordingly.

2.14. Ethics

Analyses of public GEO datasets used de-identified public data and did not require additional ethics approval. Donor-derived blood collection for ex vivo immune co-culture assays was performed after written informed consent under institutionally approved protocols in accordance with the Declaration of Helsinki. Consent covered the use of de-identified blood samples for functional immune assays. Because the

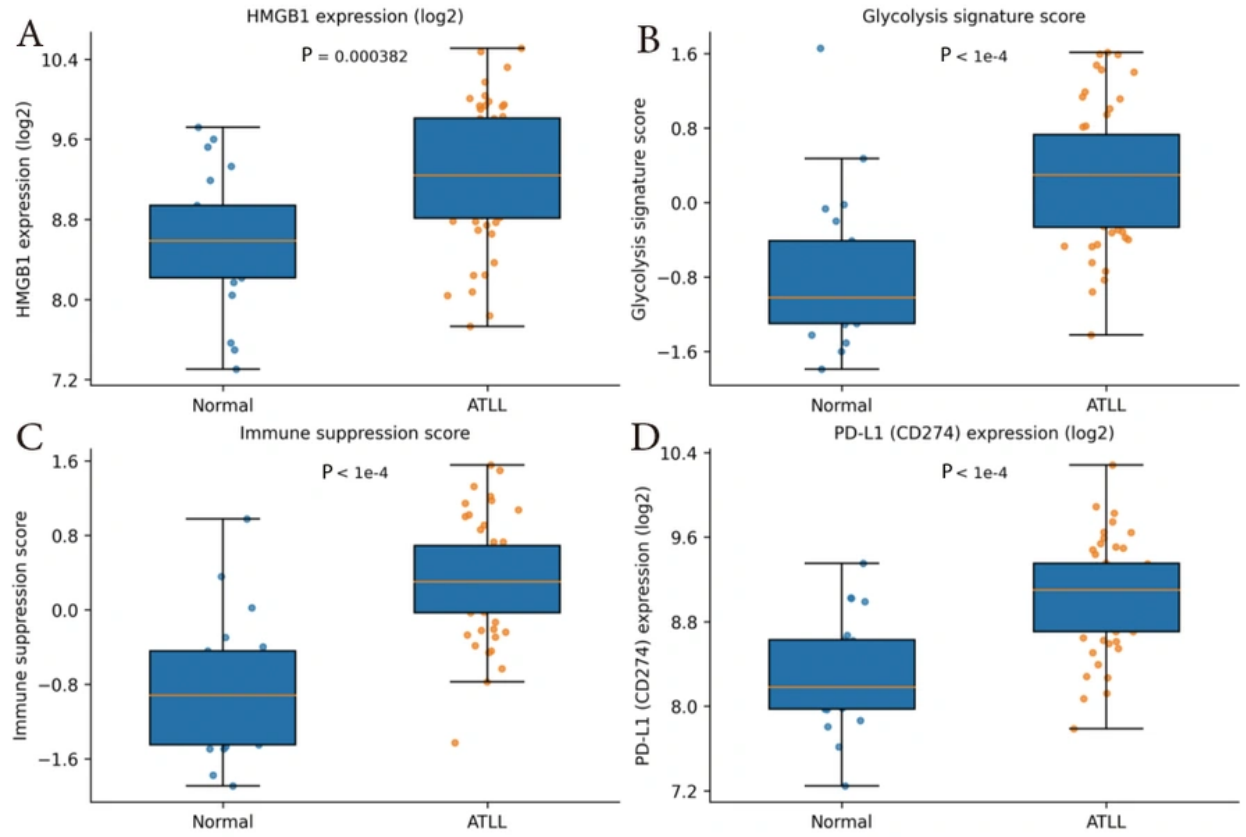

Figure 2. HMGB1, glycolysis, and immune-inhibitory signatures are elevated in adult T-cell leukemia/lymphoma (ATLL). A, HMGB1 log2 expression; B, glycolysis signature score; C, immune-inhibitory signature score; D, CD274 (programmed death-ligand 1 [PD-L1]) log2 expression. Each boxplot shows the median, interquartile range, and 1.5 × interquartile range whiskers with individual samples overlaid. ATLL, n = 52; normal controls, n = 21. P values were calculated with two-sided Mann-Whitney U tests. Positive signature values indicate above-cohort-average enrichment after within-cohort standardization.

study did not involve an interventional clinical trial, clinical trial registration was not applicable.

3. Results

3.1. HMGB1 and Two Predefined Signatures Are Elevated in Adult T-Cell Leukemia/Lymphoma Patient Samples

In GSE33615, HMGB1 expression was higher in ATLL than in normal CD4+ T-cell controls (9.26 ± 0.68 vs 8.58 ± 0.67 log2 units; Mann-Whitney $P = 3.8 \times 10^{-4}$). The glycolysis signature score was also higher in ATLL (0.30 ± 0.72 vs -0.75 ± 0.44; $P = 4.6 \times 10^{-10}$), as was the immune-inhibitory signature score (0.42 ± 0.69 vs -1.05 ± 0.27; $P = 1.2 \times 10^{-15}$). CD274 expression was elevated in ATLL as well ($P = 2.9 \times 10^{-6}$) (Figure 2; Supplementary Table S1). Because these values arise from a single public cohort that combines diagnostic and source differences, we treat them as within-cohort associations rather than proof of cell-intrinsic causality.

3.2. Within Adult T-Cell Leukemia/Lymphoma, HMGB1 Tracks with Glycolytic and Immune-Inhibitory States

Restricting the analysis to ATLL samples, HMGB1 expression was positively associated with the glycolysis signature score (Spearman rho = 0.73, $P = 6.8 \times 10^{-10}$) and the immune-inhibitory signature score (rho = 0.74, $P = 2.8 \times 10^{-10}$). CD274 showed similar associations with glycolysis (rho = 0.67, $P = 4.4 \times 10^{-8}$) and the immune-inhibitory score (rho = 0.72, $P = 6.3 \times 10^{-10}$) (Figure 3). Directionally similar results were obtained in source-adjusted regression models, but the observational nature of the cohort and the inability to fully control for

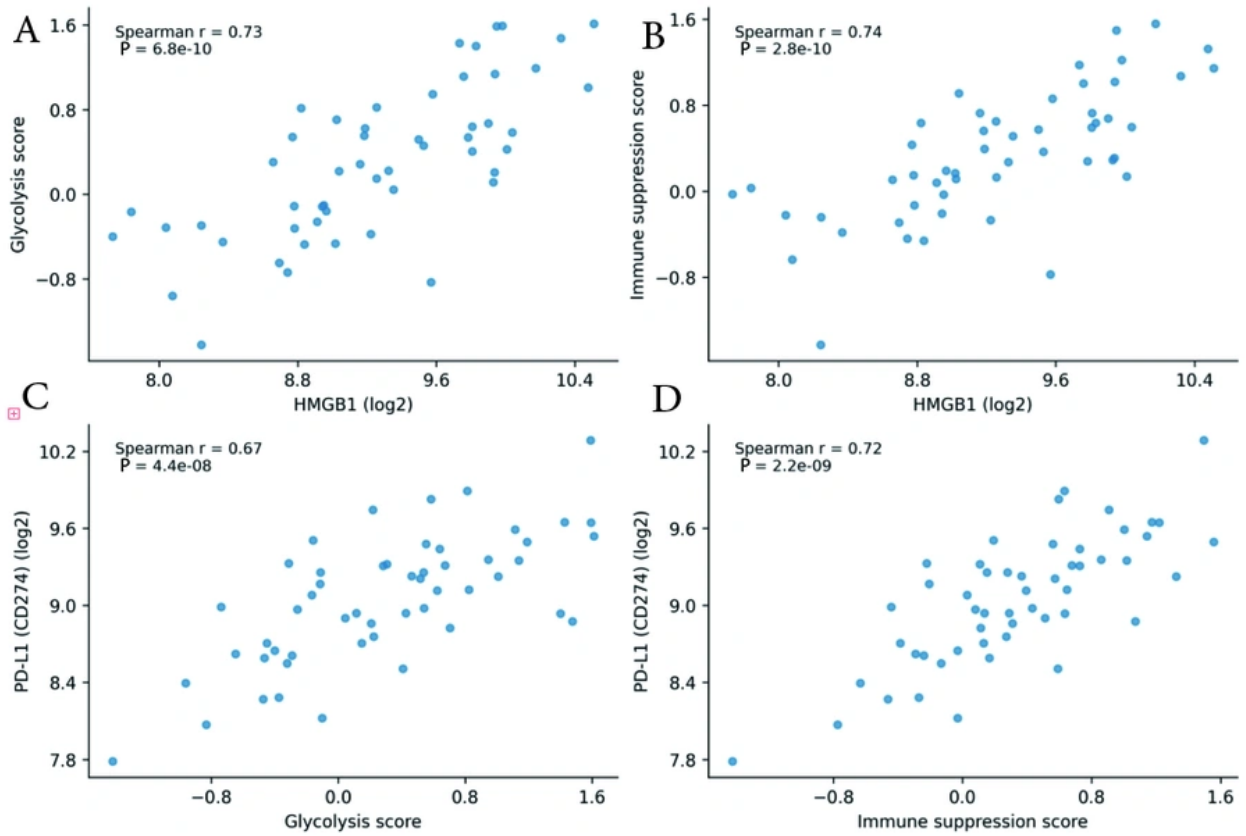

Figure 3. Correlations among HMGB1, glycolysis, immune-inhibitory signaling, and programmed death-ligand 1 (PD-L1) within adult T-cell leukemia/lymphoma (ATLL). A, HMGB1 vs glycolysis signature score; B, HMGB1 vs immune-inhibitory signature score; C, CD274 vs glycolysis signature score; D, CD274 vs immune-inhibitory signature score. Scatter plots are restricted to ATLL samples (n = 52). Correlation coefficients are Spearman rho, and two-sided P values are shown for each panel.

tumor purity or cell composition mean that these relationships should be interpreted as associative.

3.3. Tax Induction Is Accompanied by Coordinated Upregulation of HMGB1 and Related Metabolic and Checkpoint Programs

To move beyond cross-sectional associations, we analyzed a Tax on/off switch model. Relative to the Tax-off state, Tax-on samples showed higher HMGB1 expression, higher glycolysis scores, and higher immune-inhibitory/CD274 programs, consistent with a Tax-associated transcriptional shift (Supplementary Figure S1A; Supplementary Table S2). These data do not by themselves prove direct promoter regulation, but they provide directional support for the ordering tested in the mechanistic assays.

3.4. Cross-Cohort Effect-Size Concordance Supports a Shared Tax-HMGB1 Axis

Candidate-gene differential analyses across the patient cohort, Tax-switch model, and HTLV-1 comparison cohort showed concordant positive effect sizes for HMGB1 and multiple glycolysis and immune-inhibitory genes, including SLC2A1, HK2, PKM, LDHA, CD274, and LGALS9 (Table 2; Supplementary Figure S5). Although the smallest cohort had attenuated statistical power, the direction of change was conserved across all three datasets for the core axis genes, supporting a reproducible pattern rather than a single-cohort artifact.

3.5. Co-expression Modules and Single-Cell Context Identify a Tumor-Microenvironment Program Centered on HMGB1

Table 2. Cross-Cohort Differential-Expression Effect Sizes for Selected Axis Genes [a]

Gene	Patient log2FC	Patient FDR	Tax-switch log2FC	Tax-switch FDR	Cell-line log2FC	Cell-line FDR
HMGB1	0.682	1.62×10^{-3}	1.071	4.90×10^{-3}	1.083	3.14×10^{-1}
SLC2A1	0.736	1.73×10^{-4}	0.972	1.29×10^{-3}	1.073	3.17×10^{-1}
HK2	0.591	2.53×10^{-3}	0.967	1.29×10^{-3}	1.012	3.17×10^{-1}
PKM	0.766	2.93×10^{-4}	1.097	3.28×10^{-3}	0.859	3.29×10^{-1}
LDHA	0.879	1.13×10^{-4}	1.158	3.80×10^{-3}	1.083	3.17×10^{-1}
CD274	0.738	6.00×10^{-5}	0.999	3.13×10^{-3}	0.747	3.29×10^{-1}
LGALS9	0.708	2.00×10^{-5}	0.910	8.82×10^{-4}	0.684	3.79×10^{-1}

[a] Positive log2 fold-change values indicate higher expression in ATLL, Tax-on, or HTLV-I-positive samples, respectively. FDR values are Benjamini-Hochberg adjusted within each cohort. Abbreviations: FC, fold change; FDR, false discovery rate.

WGCNA identified a glycolysis-associated blue module and an immune-inhibitory brown module, both strongly correlated with HMGB1 expression in the bulk ATLL cohort. The blue module correlated with HMGB1 (rho = 0.83, $P = 1.9 \times 10^{-19}$), glycolysis score (rho = 0.98, $P = 1.3 \times 10^{-53}$), and immune-inhibitory score (rho = 0.96, $P = 1.9 \times 10^{-41}$). The brown module showed similarly strong relationships with HMGB1 (rho = 0.80, $P = 1.5 \times 10^{-17}$), glycolysis (rho = 0.97, $P = 4.4 \times 10^{-44}$), and immune-inhibitory signaling (rho = 0.98, $P = 3.5 \times 10^{-51}$) (Supplementary Figure S2A; Supplementary Tables S5-S7). In the supporting single-cell dataset, glycolysis-related expression was highest in malignant T cells, whereas HMGB1 and CD274 were especially prominent in myeloid cells and also present in malignant T cells (Supplementary Figure S2B; Supplementary Tables S8-S9). This pattern is consistent with combined tumor-intrinsic and microenvironmental contributions and argues against a purely single-compartment interpretation of the bulk correlations.

3.6. Tax Directly Activates the HMGB1 Promoter Through a C/EBP-Like Element

We next tested whether Tax directly regulates HMGB1 transcription. Tax increased the full-length HMGB1 reporter from 1.00 ± 0.17 to 2.64 ± 0.16 relative units ($P = 2.8 \times 10^{-4}$) and increased the truncated reporter from 0.96 ± 0.20 to 1.93 ± 0.26 relative units ($P = 8.4 \times 10^{-3}$). In contrast, mutation of the C/EBP-like motif largely abolished Tax responsiveness (0.90 ± 0.10 vs 1.07 ± 0.10; P = 0.117 for Tax plus vs Tax minus; $P = 3.7 \times 10^{-4}$ for mutant Tax plus vs wild-type full-length Tax plus) (Supplementary Figure S3A; Supplementary Table S10). ChIP-qPCR further showed Tax enrichment at the HMGB1 promoter interval -1163 to -975 (9.74 ± 2.42-fold) relative to a distal negative-control region (0.91 ± 0.01-fold; P = 0.024), while the NFKBIA promoter behaved as a positive-control Tax target (23.02 ± 4.03-fold) (Supplementary Figure S3B; Supplementary Table S11). Together, these data support direct transcriptional engagement of the HMGB1 promoter by Tax and identify the C/EBP-like element as a required component of the responsive region.

3.7. HMGB1 Lies Upstream of Tax-Associated Glycolytic Remodeling

Tax activation increased extracellular lactate from 5.07 ± 0.09 mM in Tax-off siCtrl cells to 12.67 ± 1.05 mM in Tax-on siCtrl cells ($P = 6.0 \times 10^{-3}$). Tax also increased ECAR from 39.74 ± 3.93 to 87.30 ± 7.36 mpH/min ($P = 2.1 \times 10^{-3}$) and glucose uptake from $1.07 \times 10^4 \pm 1.79 \times 10^2$ to $1.66 \times 10^4 \pm 8.39 \times 10^2$ arbitrary units ($P = 5.0 \times 10^{-3}$) (Supplementary Figure S3C-S3D; Supplementary Table S12). HMGB1 knockdown significantly reduced lactate (7.22 ± 0.54 mM; $P = 4.2 \times 10^{-3}$ vs Tax-on siCtrl), ECAR (54.11 ± 1.64 mpH/min; $P = 1.3 \times 10^{-2}$), and glucose uptake ($1.23 \times 10^4 \pm 1.42 \times 10^3$ arbitrary units; $P = 1.6 \times 10^{-2}$). Re-expression of HMGB1 partially restored lactate (10.37 ± 0.83 mM; $P = 8.2 \times 10^{-3}$ vs Tax-on siHMGB1) and ECAR (69.37 ± 5.63 mpH/min; $P = 3.4 \times 10^{-2}$), and it returned glucose uptake to the Tax-on range ($1.70 \times 10^4 \pm 1.75 \times 10^3$ arbitrary units; $P = 2.4 \times 10^{-2}$ vs Tax-on siHMGB1; P = 0.79 vs Tax-on siCtrl). These rescue data place HMGB1 upstream of the metabolic phenotype rather than acting only as a parallel correlate.

3.8. HMGB1-Dependent Lactate Output Accompanies a Tax-Associated Immune-Evasion Phenotype

Tax-on target cells expressed more surface PD-L1 than Tax-off controls (874.7 ± 71.6 vs 344.2 ± 42.0 MFI; paired $P = 1.6 \times 10^{-4}$) and more surface Galectin-9 (876.5 ± 78.4 vs 410.1 ± 52.7 MFI; paired $P = 4.4 \times 10^{-4}$). HMGB1 knockdown lowered PD-L1 to 553.7 ± 28.7 MFI ($P = 1.0 \times 10^{-3}$ vs Tax-on siCtrl) and Galectin-9 to 601.5 ± 94.2 MFI ($P = 7.7 \times 10^{-3}$) (Supplementary Figure S3E; Supplementary Tables S15-S16). In donor-matched cytotoxic co-cultures, Tax-on targets were killed less efficiently than Tax-off targets (24.9% ± 3.6% vs 47.9% ± 2.4%; paired $P = 1.7 \times 10^{-4}$) and induced less IFN-gamma release (141.4 ± 30.5 vs 268.4 ± 11.2 pg/mL; paired $P = 2.5 \times 10^{-4}$). HMGB1 knockdown increased killing to 38.6% ± 4.3% ($P = 4.5 \times 10^{-4}$ vs Tax-on siCtrl) and IFN-gamma to 215.2 ± 20.0 pg/mL ($P = 9.3 \times 10^{-3}$) (Supplementary Figure S3F; Supplementary Table S15). PD-L1 blockade improved killing of Tax-on targets to 43.5% ± 2.4% ($P = 2.1 \times 10^{-5}$ vs Tax-on siCtrl), whereas lactate inhibition increased killing to 38.0% ± 4.5% ($P = 1.7 \times 10^{-3}$) and reduced PD-L1 and Galectin-9 MFI (PD-L1, $P = 2.3 \times 10^{-2}$; Galectin-9, $P = 2.8 \times 10^{-3}$). These interventions did not fully normalize the phenotype, indicating that lactate-sensitive checkpoint regulation contributes to, but does not completely explain, the Tax-HMGB1 immune-evasion program.

4. Discussion

By combining public ATLL transcriptomes with promoter-level and functional experiments, we found that Tax directly engages the HMGB1 promoter and that HMGB1 is required for a substantial part of the Tax-associated glycolytic and immune-evasion phenotype. The patient datasets support this axis at the level of association: HMGB1 tracked with glycolytic and immune-inhibitory programs in ATLL, and those patterns were directionally concordant across independent cohorts. The causal claims in this study therefore rest primarily on the Tax-switch, reporter, ChIP-qPCR, knockdown, and rescue experiments rather than on the public cohorts alone (1, 4 - 6, 9).

The strongest mechanistic evidence comes from the promoter assays. Tax increased activity of two HMGB1 promoter constructs that retained the responsive interval, and mutation of the C/EBP-like motif sharply reduced that response. Promoter enrichment in ChIP-qPCR, together with the positive-control NFKBIA locus and distal negative-control region, supports specific promoter engagement rather than global chromatin activation alone. These data position HMGB1 as a bona fide Tax-responsive transcriptional node in this system (4).

The functional perturbation data place HMGB1 upstream of metabolic remodeling and link that metabolic shift to immune phenotype. HMGB1 knockdown reduced lactate, ECAR, glucose uptake, PD-L1, Galectin-9, and cytotoxic resistance, whereas HMGB1 re-expression restored metabolic output. Lactate inhibition also reduced checkpoint expression and improved killing, supporting a lactate-sensitive component downstream of HMGB1. At the same time, the partial rather than complete rescue by PD-L1 blockade or lactate inhibition indicates that parallel Tax-driven programs almost certainly operate in ATLL cells. We therefore interpret the Tax-HMGB1-lactate-checkpoint sequence as a supported but not exclusive pathway (5, 8, 9).

HMGB1 biology is compartment-dependent, and our data more directly support an intracellular transcriptional role than an extracellular cytokine-like one. The promoter and knockdown experiments interrogate cell-intrinsic HMGB1, whereas we did not directly quantify secreted HMGB1, its redox state, or receptor engagement in co-culture supernatants. The single-cell data further suggest that HMGB1 and PD-L1 are distributed across both malignant T cells and myeloid populations, consistent with combined tumor and microenvironmental contributions. Future work should therefore distinguish nuclear HMGB1-dependent transcription from extracellular HMGB1 signaling by measuring secretion, neutralizing extracellular HMGB1, and testing receptor-specific blockade (6, 7).

Several limitations should bound interpretation. First, the public bulk cohorts differ in platform, source material, and disease composition; accordingly, we restricted cross-cohort inference to within-cohort effect sizes and standardized scores and treat those data as associative. Second, tumor purity, cell mixture, and ATLL subtype cannot be fully resolved in the bulk analyses. Third, the co-culture model uses healthy-donor effector cells and a simplified ex vivo interaction window; it captures cytotoxic sensitivity but not the full chronic tumor microenvironment. Fourth, although we expanded the reporting of derived scores, source data, and analysis metadata in the revised submission, a permanent public deposition of the complete workflow should remain a priority for long-term reproducibility. Within those bounds, the convergence of direct promoter assays, HMGB1 perturbation and rescue, and

donor-matched functional readouts supports the biological relevance of the Tax-HMGB1 axis.

Overall, our data support a model in which Tax directly activates HMGB1 transcription, HMGB1 amplifies glycolytic flux and lactate output, and this state contributes to a checkpoint-rich, cytotoxicity-resistant phenotype. This framework links viral transcriptional control to immunometabolic adaptation and provides a rationale for combining metabolic and immune-directed interventions in ATLL.

5. Conclusion

In summary, the revised integrated analyses and functional experiments identify HMGB1 as a direct Tax-responsive transcriptional target and as an upstream regulator of glycolytic and immune-evasion phenotypes in ATLL models. The public patient cohorts support the same axis at the level of association, while the mechanistic experiments define its directionality more directly. Targeting HMGB1-linked metabolic and checkpoint pathways may therefore offer complementary leverage points for restoring anti-tumor immunity in ATLL.

Supplementary Material

Supplementary material(s) is available here [To read supplementary materials, please refer to the journal website and open PDF/HTML].

Footnotes

AI Use Disclosure: The authors declare that no generative AI tools were used in the creation of this article.

Authors' Contribution: Study concept and design: H.G. and R.X.; Acquisition of data: R.L. and S.Z.; Analysis and interpretation of data: R.L., S.Z., and H.G.; Drafting of the manuscript: R.L.; Critical revision of the manuscript for important intellectual content: H.G. and R.X.; Statistical analysis: R.L. and S.Z.; Administrative, technical, and material support: S.Z. and R.X.; Study supervision: H.G. and R.X. All authors read and approved the final manuscript.

Conflict of Interests Statement: The authors declare no conflict of interests.

Data Availability: All public transcriptome data analyzed in this study are available from GEO under accession numbers GSE33615, GSE10508, GSE17718, and GSE195674. Figure-level source data and expanded tables are provided in Supplementary_Tables.xlsx. A versioned reproducibility package included with this revised submission (Reproducibility_Package_v1.0.zip) contains the harmonized study manifest, predefined gene sets, source-data exports, and analysis scripts used to regenerate the reported summary statistics and figure-level tables from the deposited source tables.

Funding/Support: This study was supported by the Fujian Natural Science Foundation Project, "Research on the Application of Aptamer-Molecular Interaction Technology in the Diagnosis and Treatment of HTLV-1 Virus Infection" (Grant No. 2021J01265).

Informed Consent: Analyses of public transcriptomes used de-identified public data. Donor-derived blood collection for ex vivo assays was performed after written informed consent under institutionally approved protocols.

References

1. El Hajj H, Bazarbachi A. Interplay between innate immunity and the viral oncoproteins Tax and HBZ in the pathogenesis and therapeutic response of HTLV-1 associated adult T cell leukemia. *Frontiers in Immunology*. 2022;**13**. 957535. [PubMed ID: 35935975]. [PubMed Central ID: PMC9352851]. https://doi.org/10.3389/fimmu.2022.957535.
2. Bellon M, Nicot C. HTLV-1 Tax Tug-of-War: Cellular Senescence and Death or Cellular Transformation. *Pathogens*. 2024;**13**(1):87. [PubMed ID: 38276160]. [PubMed Central ID: PMC10820833]. https://doi.org/10.3390/pathogens13010087.
3. Hleihel R, Skayneh H, de Thé H, Hermine O, Bazarbachi A. Primary cells from patients with adult T cell leukemia/lymphoma depend on HTLV-1 Tax expression for NF-κB activation and survival. *Blood Cancer Journal*. 2023;**13**(1):67. [PubMed ID: 37137914]. [PubMed Central ID: PMC10156663]. https://doi.org/10.1038/s41408-023-00841-7.
4. Shirasawa M, Nakajima R, Zhou Y, Fikriyanti M, Iwanaga R, Bradford A. Transcriptional Activation Mechanisms and Target Genes of the Oncogene Product Tax of Human T-Cell Leukemia Virus Type 1. *Genes*. 2025;**16**(10):1221. [PubMed ID: 41153438]. [PubMed Central ID: PMC12564054]. https://doi.org/10.3390/genes16101221.
5. Huang L, Chen X, Yan M, Xiang Z, Wu J. Lactate and lactylation in breast cancer: current understanding and therapeutic opportunities. *Cancer Biol Med*. 2025;**22**(7):789-805. [PubMed ID: 40671416]. [PubMed Central ID: PMC12302272]. https://doi.org/10.20892/j.issn.2095-3941.2025.0173.
6. Hubert P, Roncarati P, Demoulin S. Extracellular HMGB1 blockade inhibits tumor growth through profoundly remodeling immune microenvironment and enhances checkpoint inhibitor-based immunotherapy. *Journal for Immunotherapy of Cancer*. 2021;**9**(3). e001966. [PubMed ID: 33712445]. [PubMed Central ID: PMC7959241]. https://doi.org/10.1136/jitc-2020-001966.
7. Joo E, Bae J, Park J, Bang Y, Han J, Gulati N. Deconvolution of Adult T-Cell Leukemia/Lymphoma With Single-Cell RNA-Seq Using Frozen Archived Skin Tissue Reveals New Subset of Cancer-Associated Fibroblast. *Frontiers in Immunology*. 2022;**13**. 856363. [PubMed ID: 35464471]. [PubMed Central ID: PMC9021607]. https://doi.org/10.3389/fimmu.2022.856363.
8. Jalili-Nik M, Soltani A, Mashkani B, Rafatpanah H, Hashemy S. PD-1 and PD-L1 inhibitors foster the progression of adult T-cell

Leukemia/Lymphoma. *International Immunopharmacology*. 2021;**98**. 107870. [PubMed ID: 34153661]. https://doi.org/10.1016/j.intimp.2021.107870.

9. Chiba M, Shimono J, Suto K. Whole-genome CRISPR screening identifies molecular mechanisms of PD-L1 expression in adult T-cell leukemia/lymphoma. *Blood*. 2024;**143**(14):1379-1390. [PubMed ID: 38142436]. [PubMed Central ID: PMC11033594]. https://doi.org/10.1182/blood.2023021423.
10. Chen Y, McCarthy D, Ritchie M. edgeR v4: powerful differential analysis of sequencing data with expanded functionality and improved support for small counts and larger datasets. *Nucleic Acids Research*. 2025;**53**(2). gkaf018. [PubMed ID: 39844453]. [PubMed Central ID: PMC11754124]. https://doi.org/10.1093/nar/gkaf018.